

# $^{13}\text{CO}$ 1–0 imaging of the Medusa merger, NGC 4194

## Large scale variations in molecular cloud properties

S. Aalto<sup>1</sup>, R. Beswick<sup>2</sup>, and E. Jütte<sup>3</sup>

<sup>1</sup> Department of Earth and Space Sciences, Chalmers University of Technology, Onsala Observatory, 439 94 Onsala, Sweden  
e-mail: saalto@chalmers.se

<sup>2</sup> Jodrell Bank Centre for Astrophysics, School of Physics and Astronomy, The University of Manchester Oxford Road, Manchester M13 9PL, UK

<sup>3</sup> University of Bochum, Department of Astronomy, 44780 Bochum, Germany

Received 20 October 2009 / Accepted 13 July 2010

### ABSTRACT

**Aims.** Studying molecular gas properties in merging galaxies gives important clues to the onset and evolution of interaction-triggered starbursts. The  $\frac{^{12}\text{CO}}{^{13}\text{CO}}$  line intensity ratio can be used as a tracer of how dynamics and star formation processes impact the gas properties. The Medusa merger (NGC 4194) is particularly interesting to study since its  $\frac{L_{\text{FIR}}}{L_{\text{CO}}}$  ratio rivals that of ultraluminous galaxies (ULIRGs), despite the comparatively modest luminosity, indicating an exceptionally high star formation efficiency (SFE) in the Medusa merger. **Methods.** High resolution OVRO (Owens Valley Radio Observatory) observations of the  $^{13}\text{CO}$  1–0 have been obtained and compared with matched resolution OVRO  $^{12}\text{CO}$  1–0 data to investigate the molecular gas cloud properties in the Medusa merger.

**Results.** Interferometric observations of  $^{12}\text{CO}$  and  $^{13}\text{CO}$  1–0 in the Medusa (NGC 4194) merger show the  $\frac{^{12}\text{CO}}{^{13}\text{CO}}$  1–0 intensity ratio ( $\mathcal{R}$ ) increases from normal, quiescent values (7–10) in the outer parts ( $r > 2$  kpc) of the galaxy to high (16 to  $>40$ ) values in the central ( $r < 1$  kpc) starburst region. In the central two kpc there is an east-west gradient in  $\mathcal{R}$  where the line ratio changes by more than a factor of three over  $5''$  (945 pc). The integrated  $^{13}\text{CO}$  emission peaks in the north-western starburst region while the central  $^{12}\text{CO}$  emission is strongly associated with the prominent crossing dust-lane.

**Conclusions.** We discuss the central east-west gradient in  $\mathcal{R}$  in the context of gas properties in the starburst and the central dust lane. We suggest that the central gradient in  $\mathcal{R}$  is mainly caused by diffuse gas in the dust lane. In this scenario, the actual molecular mass distribution is better traced by the  $^{13}\text{CO}$  1–0 emission than the  $^{12}\text{CO}$ . The possibilities of temperature and abundance gradients are also discussed. We compare the central gas properties of the Medusa to those of other minor mergers and suggest that the extreme and transient phase of the Medusa star formation activity has similar traits to those of high-redshift galaxies.

**Key words.** galaxies: evolution – galaxies: individual: NGC 4194 – galaxies: starburst – galaxies: active – radio lines: ISM – ISM: molecules

## 1. Introduction

Studying the molecular cloud properties in starburst, active and interacting galaxies is important in order to understand the feedback mechanisms between star formation, dynamics and the interstellar medium. Important probes of cloud properties include molecules such as HCN,  $\text{HCO}^+$  and HNC (e.g. Krips et al. 2008; Graciá-Carpio et al. 2008; Imanishi et al. 2004; Gao & Solomon 2004; Aalto et al. 2002) that trace the dense ( $n \gtrsim 10^4 \text{ cm}^{-3}$ ) star forming phase of the molecular gas.

Alternatively, to study the bulk properties of the molecular gas one can use the ratio between  $^{12}\text{CO}$  and its isotopomer  $^{13}\text{CO}$ . Globally, there is a correlation between the  $^{12}\text{CO}/^{13}\text{CO}$  1–0 ratio ( $\mathcal{R}$ ) and the FIR  $f(60 \mu\text{m})/f(100 \mu\text{m})$  flux ratio (e.g. Young & Sanders 1986; Aalto et al. 1995). The extreme values of  $\mathcal{R}$  (i.e.  $\mathcal{R} > 20$ ) generally occur in luminous merging galaxies with large dust temperatures (e.g. Aalto et al. 1995; Glenn & Hunter 2001). Within galaxies there is a general trend of increasing  $\mathcal{R}$  towards the central region where the gas is warmer and denser (e.g. Wall et al. 1993; Aalto et al. 1995; Paglione et al. 2001).

Both high kinetic temperatures and large turbulent line widths will decrease the optical depth ( $\tau$ ), of the  $^{12}\text{CO}$  and  $^{13}\text{CO}$  1–0 lines and thus elevate the line ratio  $\mathcal{R}$ . Therefore,

information on the spatial variation of  $\mathcal{R}$  can be used to identify regions of extreme or unusual physical conditions in the molecular gas – and global values can help classify galaxies. Aalto et al. (1995) suggested some general diagnostics of the cloud conditions and environment based on global values of  $\mathcal{R}$ :

- small ratios,  $\mathcal{R} \approx 6$  are an indication of a normal Galactic disc population of clouds dominated by cool, self-gravitating giant molecular clouds (GMCs);
- intermediate ratios  $10 \lesssim \mathcal{R} \lesssim 15$  are associated with the inner regions of normal starburst galaxies where the gas is warmer and denser than in the disc;
- the extreme values  $\mathcal{R} > 20$  seem to originate in warm, turbulent, high pressure gas in the centres of luminous mergers with highly compact molecular distributions and gas surface densities in excess of  $10^4 M_{\odot} \text{ pc}^{-2}$  – two orders of magnitude higher than in typical Milky Way GMCs. Large surface densities require high pressures in hydrostatic equilibrium and low density ( $n < 10^3 \text{ cm}^{-3}$ ) –  $^{12}\text{CO}$  emitting – gas must be supported by large turbulent line widths ( $P \propto n(\delta V)^2$ ). Thus,  $\tau_{\text{CO}}$  can be reduced to moderate ( $\approx 1$ ) values, resulting in large  $\mathcal{R}$ .

More recent studies show that high values of  $\mathcal{R}$  also occur more locally in less extreme galaxies. [Tosaki et al. \(2002\)](#) find this in the spiral arms of M 51 and [Meier & Turner \(2004\)](#) in the centre of the spiral galaxy NGC 6946. [Hüttemeister et al. \(2000\)](#) find large values of  $\mathcal{R}$  in the large scale bar of NGC 7479 as a result of the dynamical impact of a density wave on gas properties.

The nearby merger NGC 4194 – the Medusa merger – belongs to a class of lower luminosity ( $L_{\text{FIR}} = 8.5 \times 10^{10} L_{\odot}$  at  $D = 39$  Mpc) E+S mergers ([Aalto & Hüttemeister 2000](#); [Manthey et al. 2008](#)), an order of magnitude fainter than well known ultra luminous galaxies (ULIRGs ( $L_{\text{FIR}} \gtrsim 10^{12} L_{\odot}$ )) such as Arp 220. The Medusa has an elevated value of  $\mathcal{R}$  ( $\approx 20$ ) (e.g. [Aalto et al. 1991](#); [Casoli et al. 1992](#); [Glenn & Hunter 2001](#)), but in contrast to the more luminous high- $\mathcal{R}$  mergers, NGC 4194 has a relatively extended (2 kpc) starburst region (e.g. [Armus et al. 1990](#); [Prestwich et al. 1994](#)) and [Aalto & Hüttemeister \(2000\)](#) found that the molecular gas was also distributed on the comparatively large scale of  $25''$  (4.7 kpc), despite its advanced stage of merger. Due to the linear extent of the molecular gas and relative proximity of the Medusa merger, it is possible to spatially resolve the relative distributions of  $^{12}\text{CO}$  and  $^{13}\text{CO}$  and hence allow the investigation of the underlying causes of the elevated  $\mathcal{R}$  values observed in this galaxy. The Medusa starburst is particularly interesting to study since its  $\frac{L_{\text{FIR}}}{L_{\text{CO}}}$  ratio of 163 rivals that of ULIRGs (for example Arp 220 with a  $\frac{L_{\text{FIR}}}{L_{\text{CO}}}$  of 210), despite the comparatively modest luminosity, indicating an exceptionally high star formation efficiency (SFE) in the Medusa merger. [Gao & Solomon \(2004\)](#) find that for galaxies with  $L_{\text{FIR}} \lesssim 10^{11} L_{\odot}$  the  $\frac{L_{\text{FIR}}}{L_{\text{CO}}}$  ratio is typically 33. At higher luminosity they find that  $\frac{L_{\text{FIR}}}{L_{\text{CO}}}$  instead increases to 100–300. [Gao & Solomon \(2004\)](#) suggest that, in contrast to CO, the  $\frac{L_{\text{FIR}}}{L_{\text{HCN}}}$  ratio is independent of luminosity with  $\frac{L_{\text{FIR}}}{L_{\text{HCN}}} = 900$ . Interestingly the Medusa deviates significantly from this HCN correlation with a  $\frac{L_{\text{FIR}}}{L_{\text{HCN}}} \gtrsim 4075$  based on upper limits from [Aalto & Hüttemeister \(2000\)](#). Further discussion of the underlying causes of this discrepancy are presented in [Aalto & Hüttemeister \(2000\)](#).

We have imaged NGC 4194 in the  $^{13}\text{CO}$  1–0 line with the Owens Valley Radio Observatory (OVRO) millimetre array. Our aim was to compare the distribution of the  $^{12}\text{CO}$  and  $^{13}\text{CO}$  emission within the galaxy and to see how it relates to star formation, gas surface density and dynamics. In Sects. 2 and 3 we discuss the observations and results. In Sect. 4 we discuss the  $\mathcal{R}$  line ratio variations within the Medusa merger in terms of warm gas in the starburst region and possible diffuse gas in the central dust lane. Future observational tests for these proposed scenarios are suggested.

## 2. Observations

We have obtained maps of  $^{13}\text{CO}$  1–0 using the Caltech six-element OVRO millimeter array. Two tracks were taken in the low resolution configuration in April 2000. The naturally weighted synthesised beam size is  $4''.56 \times 3''.98$  ( $861 \times 752$  pc for  $D = 39$  Mpc) and the beam position angle (BPA) is  $-40^\circ$ .

System temperatures were 500–600 K. The quasar 1150+497 was used for phase calibration and Neptune and Uranus for absolute flux calibration. The digital correlator, centred at  $V_{\text{LSR}} = 2560$  km s $^{-1}$ , provided a total velocity coverage of 1170 km s $^{-1}$ . Data were binned to 4 MHz resolution, corresponding to 11 km s $^{-1}$ , and to construct the map, the resolution was reduced to 44 km s $^{-1}$ . The sensitivity of this map is 3 mJy beam $^{-1}$  channel $^{-1}$ , corresponding to 0.014 K channel $^{-1}$ .

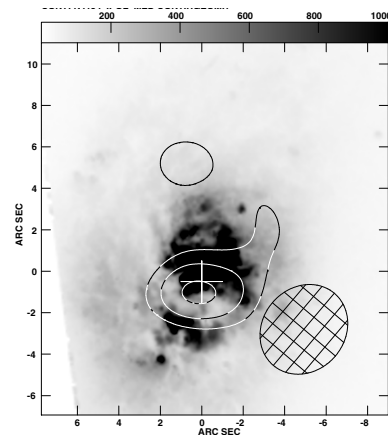


**Fig. 1.** The 110 GHz continuum of NGC 4194 overlaid on an *HST* WFPC2 image. The contours are:  $0.9 \times (-3, 3, 4, 5)$  mJy beam $^{-1}$ . Rms in the map is 1 mJy beam $^{-1}$  thus the first contour is at  $2.7\sigma$ . The peak flux density is 4.6 mJy beam $^{-1}$ . The cross marks the position of the 1.4 GHz continuum ([Condon et al. 1990](#)). Hatched ellipse indicate beam size and orientation.

### 2.1. Continuum subtraction

Using the AIPS task IMLIN we fitted continuum to the line-free channels and subtracted from the cleaned map. The resulting continuum map is presented in Fig. 1 and the flux density and position in Table 1. The 1.4 GHz continuum position of [Condon et al. \(1990\)](#) agree within  $0''.4$  with the 110 GHz position which is within the positional errors of the  $^{13}\text{CO}$  map. The 1.4 GHz radio continuum emission is dominated by synchrotron emission resulting primarily from star-formation, along with a small contribution from the compact core ([Beswick et al. 2005](#); [Condon et al. 1990](#)). The 110 GHz emission (see Fig. 1) is coincident with the area of highest dust obscuration observed in the optical. This emission is tracing the thermal emission from dust in this region illuminated by ongoing star-formation. This is consistent with the alignment in the 110 and 1.4 GHz continuum positions observed.

### 2.2. Alignment of the data

Both the  $^{12}\text{CO}$  and  $^{13}\text{CO}$  observations were made using the same instrument and employing identical gain and passband calibrators, thus minimising potential misalignments due to instrumental effects. Furthermore, the 110 GHz continuum extracted from the  $^{13}\text{CO}$  data set is positionally coincident with the 1.4 GHz continuum (see Sect. 2.1) suggesting that there are no systematic errors in the positions of the  $^{13}\text{CO}$  data set. We also note that the shift between  $^{12}\text{CO}$  and  $^{13}\text{CO}$  is partially caused by missing  $^{13}\text{CO}$  emission in some velocity channels (see Sect. 3.3).

## 3. Results: morphology of the $^{13}\text{CO}$ emission

### 3.1. Previous observations: the $^{12}\text{CO}$ distribution

High resolution OVRO aperture synthesis maps of the  $^{12}\text{CO}$  1–0 emission in the “Medusa” galaxy merger (NGC 4194) are presented in [Aalto & Hüttemeister \(2000\)](#). It was found that the molecular emission is surprisingly extended. The  $^{12}\text{CO}$  emission is distributed on a total scale of  $25''$  (4.7 kpc) – despite the apparent advanced stage of the merger. The complex, striking  $^{12}\text{CO}$  morphology occupies the centre and the north-eastern part

**Table 1.** Continuum and  $^{13}\text{CO}$  line results.

|  |   |
|--|---|
| Continuum <sup>a</sup>                         |   |
| position (J2000)                               | $\alpha$ : 12:14:09.66<br>$\delta$ : 54:31:35.0 |
| flux density(mJy)                              | $4.6 \pm 1$                                     |
| Line:  |   |
| peak flux density<br>(mJy beam <sup>-1</sup> ) | $25 \pm 3$                                      |
| integrated flux density <sup>b</sup>           |   |
| (Jy km s <sup>-1</sup> )                       | $3.3 \pm 0.6$ (centre)                          |
| (Jy km s <sup>-1</sup> )                       | $1.6 \pm 0.5$ (north)                           |

**Notes.** <sup>(a)</sup> A Gaussian was fitted to the continuum image. The error is  $1\sigma$  rms. The 1.4 GHz radio continuum position reported by [Condon et al. \(1990\)](#) is:  $\alpha$ : 12:14:09.66  $\delta$ : 54:31:35.5 (J2000). <sup>(b)</sup> A Gaussian was fitted to the integrated intensity map of  $^{13}\text{CO}$ . The peak integrated flux is  $1.9 \pm 0.3$  (Jy km s<sup>-1</sup>) in the centre. Thus, the central source is slightly resolved. The error is  $1\sigma$  rms.

of the main optical body (see Fig. 2 (left panel)). The extended  $^{12}\text{CO}$  flux density traces the two prominent dust lanes: one of which crosses the central region at right angles to the optical major axis, and the second which curves to the north-east and joins the base of the northern molecular tidal tail. The total molecular mass in the system is estimated to be at most  $2 \times 10^9 M_{\odot}$ , depending on which  $^{12}\text{CO}$ – $\text{H}_2$  conversion factor is applicable.

### 3.2. Integrated $^{13}\text{CO}$ 1–0 intensity

The naturally weighted,  $4''.5$  resolution,  $^{13}\text{CO}$  emission is distributed on a scale of  $8''$  (1.5 kpc) in an oval structure centred on the optically bright centre of the galaxy. There is also an off-centre  $^{13}\text{CO}$  concentration  $10''$  north of the centre. In Fig. 2 (right panel) we show the integrated  $^{13}\text{CO}$  map overlaid on a  $^{12}\text{CO}$  map smoothed to the  $^{13}\text{CO}$  resolution. Integrated- and peak flux densities are listed in Table 1.

The  $^{13}\text{CO}$  emission in the inner  $8''$  is shifted towards the north-west as compared to the  $^{12}\text{CO}$  distribution. The shift is  $2''.3$  (430 pc). Also the northern  $^{13}\text{CO}$  emission peak is shifted off the corresponding  $^{12}\text{CO}$  peak to the south-west by  $2''.5$ . In Fig. 3 (centre panel) the  $^{13}\text{CO}$  1–0 map is overlaid on an *HST* WFPC2 image. This shows that the  $^{13}\text{CO}$  emission is not tracing the central dust lane (which the  $^{12}\text{CO}$  does (left panel in Fig. 3)) but instead is shifted towards the north-west part of the starburst and towards the western dust features. The moment maps were produced through smoothing in velocity and space (3 channels, 3 pixels boxcar smoothing) and then applying a  $2\sigma$  flux cut-off (allowing both positive and negative flux levels).

### 3.3. The channel map

In Fig. 4 the channel maps of  $^{12}\text{CO}$  and  $^{13}\text{CO}$  1–0 are presented, smoothed to a resolution of  $5''$ . Compared to  $^{12}\text{CO}$ ,  $^{13}\text{CO}$ -emission is “missing” primarily in three velocity bins in the centre: 2495, 2538 and 2620 km s<sup>-1</sup>. In the first case we find  $^{13}\text{CO}$  emission  $10''$  north of the centre – despite  $^{12}\text{CO}$  in the same bin having a peak in the centre. In the second case  $^{13}\text{CO}$  emission is found only west of the centre while  $^{12}\text{CO}$  is distributed east and west of the radio peak. In the 2620 bin there is a bright  $^{12}\text{CO}$  peak in the centre which is missing in  $^{13}\text{CO}$ . In

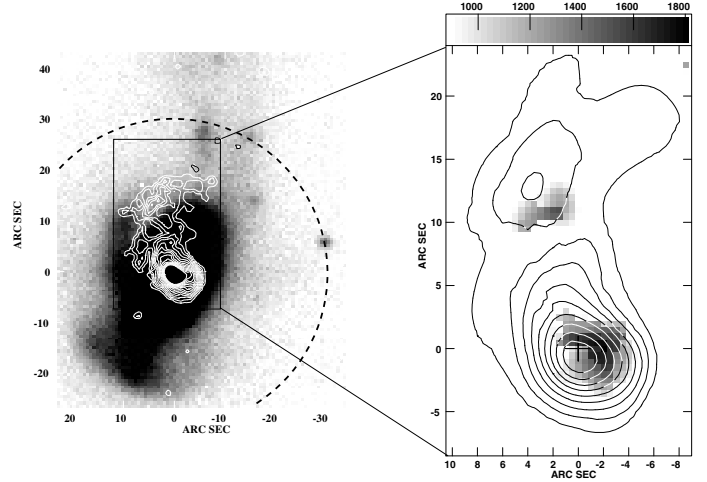


**Fig. 2.** *Left:* overlay of the  $^{12}\text{CO}$  contours (white, apart from clouds in the tail marked in black) on a greyscale, overexposed optical *R*-band image ([Mazzarella & Boroson 1993](#)). The dashed curve marks the edge of the OVRO primary beam (from [Aalto & Hüttemeister 2000](#)). *Right:* integrated  $^{13}\text{CO}$  1–0 line emission in greyscale overlaid on a  $^{12}\text{CO}$  contour map smoothed to the  $^{13}\text{CO}$  resolution of  $4''.5$ . The greyscale range is  $0.9$ – $2.0$  Jy km s<sup>-1</sup> beam<sup>-1</sup>. The CO contours are  $5.3 \times (1, 2, 3, 4, 5, 6, 7, 8)$  Jy km s<sup>-1</sup> beam<sup>-1</sup> (starting at  $6\sigma$ ). Cross indicate position of 1.4 GHz radio continuum peak (as in Fig. 1).

general, the channel maps show that there is no  $^{13}\text{CO}$  emission east, north-east of the radio continuum peak apart from a small region of emission  $10''$  north of the central region.

### 3.4. Line ratios

We find that  $\mathcal{R}$  is 7–10 in the region  $10''$  north of the centre – while in the centre it is significantly greater: ranging from 16 in the western region of the centre to  $>45$  ( $3\sigma$ ) in the eastern part of the centre where the central dust lane is making a 90 degree turn. Over a distance of  $5''$  (945 pc) the line ratio,  $\mathcal{R}$ , changes by more than a factor of 3. A map of the varying  $\mathcal{R}$  line ratios is displayed in Fig. 3 (right panel).

## 4. Discussion

The line ratio change in the Medusa occurs on scales of 0.5 to 1 kpc where the ratio goes from extreme ratios  $>40$  to more normal starburst ratios of 16. This observed gradient in  $\mathcal{R}$  is likely to be caused either by the presence of diffuse, unbound molecular gas or a temperature gradient in the ISM. In the following section we discuss each of these scenarios and compare these with observations in other galaxies.

### 4.1. Diffuse gas in the central dust lane?

Optical images of the Medusa merger are dominated by the strong absorption from several dust lanes – the most prominent one crossing the central starburst region. We suggest that the intense starburst activity is being fed by gas funnelled along the dust lane – supported by the bright  $^{12}\text{CO}$  emission associated with the dust lane(s), and the distribution and dynamics seen in the HI absorption at high resolution ([Beswick et al. 2005](#)). The central dust lane is in front of the main burst region in the east and then appears to curve into the burst region itself at the centre.

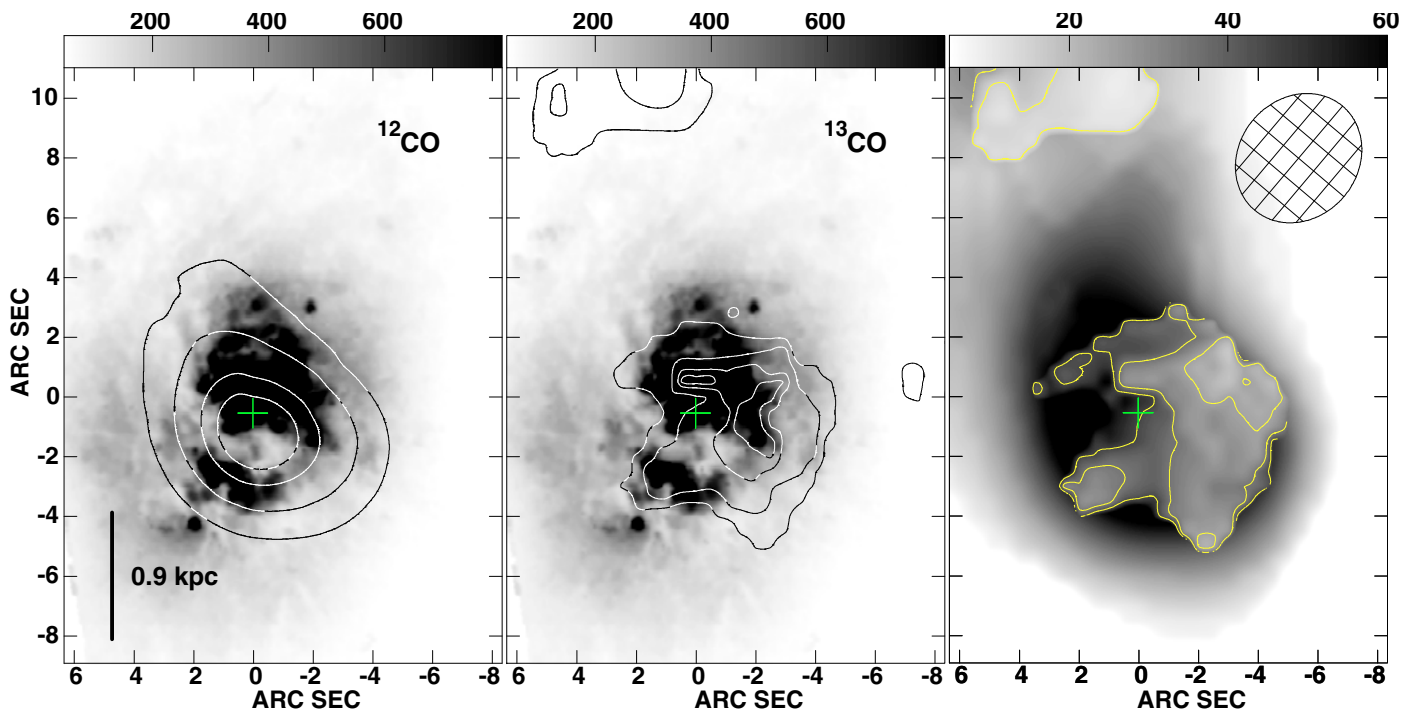


**Fig. 3.** *Left:*  $^{12}\text{CO}$  contours on a WFPC2 image zoomed in on the central region. *Centre:*  $^{13}\text{CO}$  contours on WFPC2 image. Both  $^{12}\text{CO}$  and  $^{13}\text{CO}$  contours are 40% of peak flux  $\times (1, 1.5, 2, 2.25)$ . For  $^{13}\text{CO}$  the first contour starts at  $2.5\sigma$ , for  $^{12}\text{CO}$  the first contour starts at  $24\sigma$ . *Right:* line ratio map where the greyscale ranges from light ( $\mathcal{R} = 10$ ) to dark ( $\mathcal{R} = 60$ ). Both limits and real values in greys (same scale), and the area where there are actual measures overlaid with contours (yellow). Contours are ratios  $\mathcal{R} = 15, 25, 35, 45$ . Limits are at the  $3\sigma$   $^{13}\text{CO}$  detection threshold. Please note the small pixel-size ( $0''.5$ ) of the  $^{12}\text{CO}$  and  $^{13}\text{CO}$  maps which may give the impression that there is structure beyond the actual angular resolution of the  $^{12}\text{CO}$  and  $^{13}\text{CO}$  maps.

A possible scenario is then that the molecular gas is diffuse (non self-gravitating) in the dust lane region – creating the general east-west gradient in the line ratio  $\mathcal{R}$ .

Interestingly, a comparison of the Medusa  $^{13}\text{CO}$  image and the  $\text{H}\alpha$  images of Hattori et al. (2004) show that the position of the  $\text{H}\alpha$  equivalent width ( $EW$ ) peak coincides with the regions of lower values of  $\mathcal{R}$ . The large  $EW$  is consistent with the region being an extra-nuclear star forming region. It coincides with the western radio continuum arm and the Giant Molecular Association (GMA) feature  $c$  in the high-resolution  $^{12}\text{CO}$  map (see Aalto & Hüttemeister 2000). Thus, it seems that the  $^{13}\text{CO}$  emission correlates spatially with more quiescent, spiral-arm like star formation, shifted from the dust lane and the central starburst. Note that if the  $^{12}\text{CO}$  1–0 is mainly tracing diffuse gas the  $^{13}\text{CO}$  1–0 emission is showing the real mass distribution of the molecular gas. Figure 10 of Aalto & Hüttemeister (2000) shows that the correlation between 1.4 GHz radio continuum and the central dust lane is poor – this could be a further indication of both a lack of ongoing star formation in the dust lane as well as the molecular gas potentially being diffuse in the dust lane (see for instance the discussion of  $^{12}\text{CO}$  and radio continuum in the spiral arm of M 83 by Rand et al. 1999).

#### 4.1.1. Spatial shifts in $\mathcal{R}$ in other galaxies

Even if the central region of the Medusa is more chaotic than that of a density wave spiral galaxy, and the extinction structure suggests a three-dimensional central region, it is tempting to compare the shift in  $^{12}\text{CO}$  and  $^{13}\text{CO}$  to that found in other galaxies. Tosaki et al. (2002) found a spatial shift between  $^{12}\text{CO}$  and  $^{13}\text{CO}$  1–0 emission on similar spatial scales in the southern

spiral arm of M 51. The shift seems to separate diffuse (unbound) lower density gas (as traced by  $^{12}\text{CO}$ ) from self-gravitating gas emitting the bulk of the  $^{13}\text{CO}$  line emission. Tosaki et al. (2002) suggested that there is a  $10^7$  yr time delay between the accumulation of gas by the M 51 spiral density wave and the formation of self-gravitating clouds, resulting in the  $^{13}\text{CO}$  emission being found downstream in the spiral arm where it is also spatially correlated with  $\text{H}\alpha$  emission. Meier & Turner (2004) find for NGC 6946 that the value of  $\mathcal{R}$  reaches high values of 40 away from the central starburst which they attribute to diffuse, low-density molecular gas in and behind the molecular arms.

Within the barred galaxy NGC 7479 spatial shifts between  $^{13}\text{CO}$  and  $^{12}\text{CO}$  have also been found (Hüttemeister et al. 2000). These shifts have been attributed to density-wave or bar-like dynamical effects. The similarity of these spatial shifts with those found in the Medusa may suggest similar dynamical effects may be important. In particular, the transition region between diffuse inter arm gas and self-gravitating gas in the arms of M 51 suggesting that the similar shift in the Medusa is caused by the funnelling and compression of gas towards the starburst region.

#### 4.2. Temperature gradient in the gas?

In this scenario, the elevated value of  $\mathcal{R}$  in the eastern part of the central region is caused not by diffuse molecular gas but by the gas there being warmer and denser than in the north-west. For a temperature gradient to result in elevated values of  $\mathcal{R}$  it is required that the average gas densities exceed  $3 \times 10^3 \text{ cm}^{-3}$  (since the 1–0 transition of  $^{12}\text{CO}$  and  $^{13}\text{CO}$  must be thermalised). A change of  $\mathcal{R}$  from 16 to  $>40$  can be caused by a temperature increase from 40 to 150 K in the gas (for a constant column- and

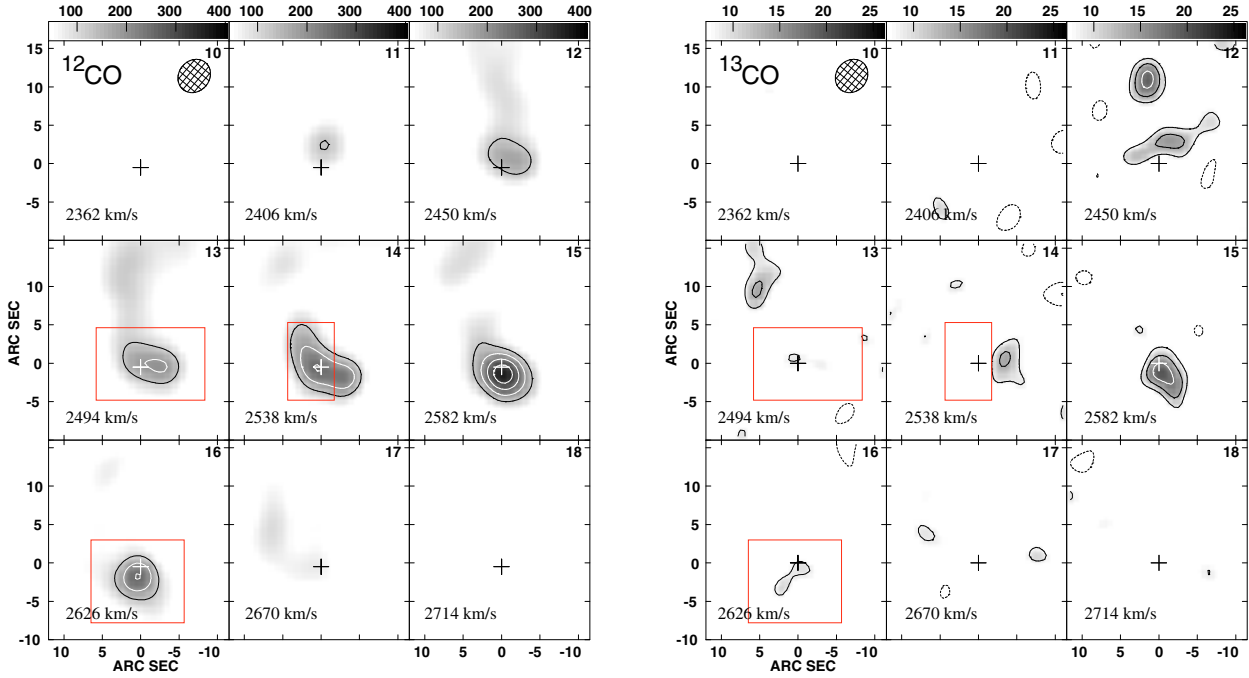


**Fig. 4.** Channel maps of  $^{12}\text{CO}$  (left) and  $^{13}\text{CO}$  (right). Boxes indicate channels of “missing”  $^{13}\text{CO}$  emission compared to  $^{12}\text{CO}$ . The  $^{12}\text{CO}$  map has been smoothed to the same resolution as  $^{13}\text{CO}$ . Intensity levels for  $^{12}\text{CO}$  and  $^{13}\text{CO}$  are same fraction of peak: 35% (–1.5, –1, 1.5, 2, 2.5) – where the peak is 360 and 25 mJy beam $^{-1}$  for the  $^{12}\text{CO}$  and  $^{13}\text{CO}$  respectively. Note that for  $^{12}\text{CO}$  a big fraction of the detected, extended flux is not shown due to the cut-off. The comparative channels maps show the position of the peak emission for  $^{12}\text{CO}$  and  $^{13}\text{CO}$ . The velocity in panel 18 = 2714 km s $^{-1}$ , panel 14 is 2538 km s $^{-1}$ , and panel 10 = 2362 km s $^{-1}$ . Increment between panels is 44 km s $^{-1}$ . Crosses indicate the 1.4 GHz radio continuum position. The beam is marked in the upper right corner of the first panel for the  $^{12}\text{CO}$  and  $^{13}\text{CO}$  channel maps. Greyscale for the  $^{12}\text{CO}$  map ranges from 50 to 400 mJy beam $^{-1}$  and for  $^{13}\text{CO}$  from 7.5 to 26 mJy beam $^{-1}$ . For the  $^{13}\text{CO}$  map the first contour corresponds to  $2.5\sigma$ .

gas density per cloud). If both the temperature and gas density is increasing towards the east then a smaller change in temperature could explain the change in  $\mathcal{R}$ . If it is filled with warm and dense gas, the dust lane would be more likely to harbour intense star formation than the rest of the central region. However, as we mentioned above, the dust lane shows no sign of elevated star formation rates, although it is potentially hidden behind large masses of dust. High resolution imaging of higher  $J$ -transition (e.g. 2–1) emission from  $^{13}\text{CO}$  and  $^{12}\text{CO}$  will allow these diffuse gas and temperature effects to be distinguished. If the faint  $^{13}\text{CO}$  1–0 emission in the eastern central part is caused by diffuse gas the  $^{13}\text{CO}$  2–1 emission should be even fainter there while the opposite is true if it is caused by a high gas temperature. This is because the 2–1 level would be more populated than the 1–0 for  $^{13}\text{CO}$  if the gas is warm – while the opposite is true if the gas is diffuse. One example where faint  $^{13}\text{CO}$  1–0 is accompanied by bright  $^{13}\text{CO}$  2–1 is the merger Arp 299 where it was suggested that the elevated value of  $\mathcal{R}$  is due to temperature effects (Aalto et al. 1999). Other studies of multi-transition  $^{13}\text{CO}$  can be found in Aalto et al. (e.g. 1995); Glenn & Hunter (e.g. 2001); Israel (e.g. 2009). Additionally, high density tracer species such as HCN or HCO $^+$  will reveal where gas of densities  $n > 10^4$  cm $^{-3}$  is located in relation to the starburst and dust lane. If the dust lane is filled with diffuse gas very little dense gas will be found there. A high resolution dust SED will reveal where hot and cold dust is in relation to the dust lane and central- and off-nuclear star formation.

*An abundance gradient:* if the physical conditions in the gas are kept constant, an elevated  $\mathcal{R}$  may be caused by a change in the  $^{12}\text{C}/^{13}\text{C}$  abundance ratio. This possibility has been discussed by Casoli et al. (e.g. 1992) as an effect of low metallicity gas being transported from the outskirts of the merger to its centre. The

starburst would then contribute to enriching the gas in  $^{13}\text{C}$ . In this scenario the gas in the dust lane has then not yet been enriched by the starburst and there is therefore an east-west and north-south age-gradient. However, abundances in NGC 4194 are found to be close to solar, and no significant metallicity gradient can be found from a study of the properties of the star forming regions (Hancock et al. 2006).

#### 4.3. The large scale gradient in $\mathcal{R}$

In the Medusa, the lowest ratios of 7–10 are found in the tail-like region north of the centre. It is not unusual to find that  $\mathcal{R}$  is decreasing away from the central region. This has been seen towards many starburst galaxies including NGC 3256, NGC 1808 and large spiral galaxies such as M 51. The gas 10'' north of the centre may therefore consist of rather ordinary cool Galactic-type GMCs. This is interesting since the gas there does not appear to be in a normal disc distribution, but rather in a shell or a tidal tail. There is no apparent star formation going on in this region and the line widths are narrow. If the gas in the central region is accumulating from the outer regions of the Medusa via the central dust lane, then our results suggest that the molecular cloud properties are normal in the outskirts, before becoming diffuse due to the funnelling of gas towards the centre and then accumulates as self-gravitating, star-forming clouds in the centre of the Medusa.

#### 4.4. The nature of the Medusa starburst

##### 4.4.1. Comparing with local minor mergers

One of the few E+S minor mergers to have its molecular medium studied is the Medusa “look-alike” NGC 4441. Based on single

dish observations of  $^{12}\text{CO}$  and  $^{13}\text{CO}$  2–1 and 1–0 Jütte et al. (2010) suggest that the molecular gas is in an unbound, diffuse state. Interestingly NGC 4441 appears to be an evolved version of the Medusa with similar morphology and luminosity and high resolution  $^{12}\text{CO}$  1–0 observations of NGC 4441 show that it traces a centrally crossing dust lane. The star formation rate of NGC 4441 is much lower than that of the Medusa – likely due to the diffuse state of its molecular medium. In this paper we suggest that a fraction of the Medusa molecular ISM may be the diffuse – it is possible that the *entire* molecular gas content of NGC 4441 is in this state. This raises interesting questions on the nature of the Medusa starburst and what it will evolve into. Perhaps it will be left with a remnant, feeble dust lane, a small reservoir of diffuse gas and only low level star formation, like NGC 4441.

#### 4.4.2. Is the star formation out of equilibrium?

Despite being a minor merger of comparatively moderate luminosity, the Medusa has an  $L_{\text{FIR}}/L_{\text{CO}}$  ratio (163) similar to those of typical ULIRGs such as Arp 220 (210) – suggesting that its SFE rivals that of the compact ULIRGs. However, the fraction of dense ( $n > 10^4 \text{ cm}^{-3}$ ) gas is significantly lower in the Medusa despite its similar SFE to ULIRGs (Aalto & Hüttemeister 2000). Aalto & Hüttemeister (2000) estimate the gas consumption time for the Medusa starburst to 40 Myr and, if a significant fraction of the molecular medium is diffuse, this time could be even shorter.

The picture becomes even more interesting when one considers that most of the ongoing star formation in the Medusa seems not to be traced by FIR or radio emission. The  $\text{H}\alpha$  SFR is found to be  $\approx 46 M_{\odot} \text{ yr}^{-1}$  (Hancock et al. 2006), while the FIR estimated SFR is  $6\text{--}7 M_{\odot} \text{ yr}^{-1}$  (Aalto & Hüttemeister 2000). (Note, that the SFR estimated from  $\text{H}\alpha$  would suggest an even more extreme SFE than the already high SFE derived from the FIR emission.) It is possible that variations in the initial mass function (IMF) can account for some of these differences (e.g. Wilkins et al. 2008), although the issue is far from resolved. Such an anomaly in the form of a flatter upper IMF *could* lead to enhanced  $\text{H}\alpha$  emission. The molecular morphology is also quite different from that of 1.4 GHz radio continuum – which is also quite different from that found from other luminous galaxies where the two distributions are usually found to coincide. The optical star formation is concentrated in knots that could be precursors to globular clusters. These knots have no clear spatial relation to either the molecular gas distribution or the continuum. *This indicates a local deviation from the Kennicutt-Schmidt relation (KS) in the Medusa that warrants further study. We suggest that the starburst of the Medusa is in an extreme transient phase of very high efficiency.*

#### 4.4.3. Comparing the Medusa to high-redshifts extreme starbursts

The Medusa merger has a number of features in common with some extreme starbursts at high- $z$  (despite its significantly lower luminosity). The starburst regions in high- $z$  systems often seem extended ( $>3$  kpc), gas consumption times are similarly short and there is a combination of ordered rotation and merger-driven random motions and inflows. More importantly, Bothwell et al. (2010) find for three  $z = 3$  ULIRGs a significant size difference between the CO distribution and star formation tracers. They find that this size difference results in the SFEs within systems

to vary by up to a factor of five. As a consequence to their results they conclude that SMGs lie significantly above the KS relation, indicating that stars may be formed more efficiently in these extreme systems than in other high- $z$  starburst galaxies. The Medusa merger is (by far) less luminous than the high- $z$  systems studied by Bothwell et al. (2010) but a careful study of the extreme starburst of the Medusa merger may lead to insights that can be applied to more distant galaxies.

## 5. Conclusions

We have obtained a high resolution map of the Medusa merger, NGC 4194, in the  $^{13}\text{CO}$  1–0 line with the OVRO array. The main conclusions we draw from this map are:

1. The  $^{13}\text{CO}$  1–0 emission is mainly distributed in the north-western part of the inner  $8''$  region. There is also an off-centre  $^{13}\text{CO}$  peak in the tail-like distribution to the north, where the  $\text{CO}/^{13}\text{CO}$  line ratios are similar to those of galactic type GMCs
2. The  $^{12}\text{CO}/^{13}\text{CO}$  1–0 line ratio,  $\mathcal{R}$ , varies on a scale of 954 pc from 16 (typical values for starburst galaxies) in the north-west to  $>40$  in the eastern part of the central region.
3. We suggest that this shift between  $^{12}\text{CO}$  and  $^{13}\text{CO}$  emission is caused by the presence of diffuse gas in a prominent dust lane crossing the eastern part of the centre. A strong density wave-like phenomenon may cause shocks (hence the dust lane) and the  $^{13}\text{CO}$  is tracing more self-gravitating gas in the post-shock region in the starburst. In this scenario, the actual molecular mass distribution is better traced by the  $^{13}\text{CO}$  1–0 emission than the  $^{12}\text{CO}$ . Alternatively, the line ratio shift is caused by temperature and density gradients in the gas. These two scenarios can be tested through imaging of  $^{13}\text{CO}$  2–1 and high density tracer molecules such as HCN and  $\text{HCO}^+$ .
4. The extreme star formation efficiency and the lack of correlation between various star formation tracers suggest that the inner region of the Medusa merger is in a highly transient phase. We predict that it will evolve into a quiescent object similar to NGC 4441, but that in its current evolutionary stage it may have some features in common with high redshift starburst galaxies.

*Acknowledgements.* This research has made use of the NASA/IPAC Extragalactic Database (NED) which is operated by the Jet Propulsion Laboratory, California Institute of Technology, under contract with the National Aeronautics and Space Administration.

## References

- Aalto, S., & Hüttemeister, S. 2000, A&A, 362, 42  
 Aalto, S., Johansson, L. E. B., Booth, R. S., & Black, J. H. 1991, A&A, 249, 323  
 Aalto, S., Booth, R. S., Black, J. H., & Johansson, L. E. B. 1995, A&A, 300, 369  
 Aalto, S., Radford, S. J. E., Scoville, N. Z., & Sargent, A. I. 1999, in *Galaxy Interactions at Low and High Redshift*, ed. J. E. Barnes, & D. B. Sanders, IAU Symp., 186, 231  
 Aalto, S., Polatidis, A. G., Hüttemeister, S., & Curran, S. J. 2002, A&A, 381, 783  
 Armus, L., Heckman, T. M., & Miley, G. K. 1990, ApJ, 364, 471  
 Beswick, R. J., Aalto, S., Pedlar, A., & Hüttemeister, S. 2005, A&A, 444, 791  
 Bothwell, M. S., Chapman, S. C., Tacconi, L., et al. 2010, MNRAS, 405, 219  
 Casoli, F., Dupraz, C., & Combes, F. 1992, A&A, 264, 55  
 Condon, J. J., Helou, G., Sanders, D. B., & Soifer, B. T. 1990, ApJS, 73, 359

- Gao, Y., & Solomon, P. M. 2004, *ApJS*, 152, 63  
Glenn, J., & Hunter, T. R. 2001, *ApJS*, 135, 177  
Graciá-Carpio, J., García-Burillo, S., Planesas, P., Fuente, A., & Usero, A. 2008, *A&A*, 479, 703  
Hancock, M., Weistrop, D., Nelson, C. H., & Kaiser, M. E. 2006, *AJ*, 131, 282  
Hattori, T., Yoshida, M., Ohtani, H., et al. 2004, *AJ*, 127, 736  
Hüttemeister, S., Aalto, S., Das, M., & Wall, W. F. 2000, *A&A*, 363, 93  
Imanishi, M., Nakanishi, K., Kuno, N., & Kohno, K. 2004, *AJ*, 128, 2037  
Israel, F. P. 2009, *A&A*, 493, 525  
Jütte, E., Aalto, S., & Hüttemeister, S. 2010, *A&A*, 509, 19  
Krips, M., Neri, R., García-Burillo, S., et al. 2008, *ApJ*, 677, 262  
Manthey, E., Hüttemeister, S., Aalto, S., Horellou, C., & Bjerkeli, P. 2008, *A&A*, 490, 975  
Mazzarella, J. M., & Boroson, T. A. 1993, *ApJS*, 85, 27  
Meier, D. S., & Turner, J. L. 2004, *AJ*, 127, 2069  
Paglione, T. A. D., Wall, W. F., Young, J. S., et al. 2001, *ApJS*, 135, 183  
Prestwich, A. H., Joseph, R. D., & Wright, G. S. 1994, *ApJ*, 422, 73  
Rand, R. J., Lord, S. D., & Higdon, J. L. 1999, *ApJ*, 513, 720  
Tosaki, T., Hasegawa, T., Shioya, Y., Kuno, N., & Matsushita, S. 2002, *PASJ*, 54, 209  
Wall, W. F., Jaffe, D. T., Bash, F. N., et al. 1993, *ApJ*, 414, 98  
Wilkins, S. M., Hopkins, A. M., Trentham, N., & Tojeiro, R. 2008, *MNRAS*, 391, 363  
Young, J. S., & Sanders, D. B. 1986, *ApJ*, 302, 680